THE JOURNAL OF PHYSICAL CHEMISTRY B

Article

pubs.acs.org/JPCB

Molecular Dynamics Simulations of Silica Nanoparticles Grafted with Poly(ethylene oxide) Oligomer Chains

Bingbing Hong and Athanassios Z. Panagiotopoulos*

Department of Chemical and Biological Engineering, Princeton University, Princeton, New Jersey 08544, United States

ABSTRACT: A molecular model of silica nanoparticles grafted with poly(ethylene oxide) oligomers has been developed for predicting the transport properties of nanoparticle organic-hybrid materials (NOHMs). Ungrafted silica nanoparticles in a medium of poly(ethylene oxide) oligomers were also simulated to clarify the effect of grafting on the dynamics of nanoparticles and chains. The model approximates nanoparticles as solid spheres and uses a united-atom representation for chains, including torsional and bond-bending interactions. The calculated viscosities from Green–Kubo relationships and temperature extrapolation are of the same order of magnitude as experimental data but show a smaller activation energy relative to real NOHMs systems. Grafted systems have higher viscosities, smaller diffusion coefficients, and slower chain dynamics than the ungrafted ones at high temperatures. At lower temperatures, grafted systems exhibit faster dynamics for both nanoparticles and chains relative to ungrafted systems, because of lower aggregation of particles and enhanced correlations between nanoparticles and chains. This agrees with the experimental observation that NOHMs have liquidlike behavior in the absence of a solvent. For both grafted and ungrafted systems at low temperatures, increasing chain length reduces the volume fraction of nanoparticles and accelerates the dynamics. However, at high temperatures, longer chains slow down nanoparticle diffusion. From the Stokes–Einstein relationship, it was determined that the coarse-grained treatment of nanoparticles leads to slip on the nanoparticle surfaces. Grafted systems obey the Stokes–Einstein relationship over the temperature range simulated, but ungrafted systems display deviations from it.

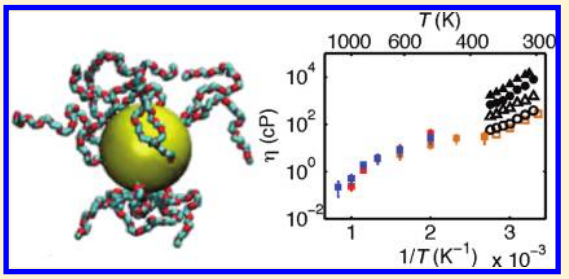

1. INTRODUCTION

Blending a small fraction of nanoparticles into a polymer matrix results in nanocomposites that can have dramatically better properties relative to the starting polymer, an improvement that is important for many engineering applications.[1−4] To prevent aggregation at high nanoparticle concentrations, the filler particles have to be surface-modified or grafted with chains compatible with the polymer matrix.[5−7] The challenge of controlling dispersion has made this an active topic of current research.[3,8−12] A different approach to organic/inorganic composites is provided by nanoparticle organic hybrid materials (NOHMs), in which all chains are covalently grafted to the particles, with no solvent molecules left. These recently developed materials have been found to exhibit liquidlike rheological behavior, even down to room temperature,[13,14] showing better processability than conventional nanocomposites. However, it is still unclear which factors control the fluidity of the materials. Grafted chains in NOHMs (500 to 5000 g/mol) typically have lower molecular weights relative to matrix chains in traditional nanoparticle polymer blends (10^5 to 10^6 g/mol). Another possible contributing factor to their fluidity is the densely grafted "corona" layers, which shield particles from each other and prevent aggregation.

Atomistic, coarse-grained, and continuum models have been used to investigate particle–polymer nanocomposites and grafted particles in free chains, in particular thermodynamics,[9−11,15−18] formation kinetics,[12,19,20] structure,[17,21−27] local chain dynamics,[17,26−29] and mechanical properties.[30−33] Simulation studies of bulk rheology are conducted in either coarse-grained or continuum level and are still limited to nanocomposites, with focus on the effect of particle shape,[33] particle–polymer interactions,[34] and particle diffusion.[12,35] In terms of other transport properties, the short-time (<400 ps) diffusion of ungrafted oligomers has been examined as a function of their distances from the nearest particle center.[17,26,27]

Few theoretical models or simulations have addressed structure and dynamics of the recently synthesized NOHMs systems. Yu et al.[36] applied density functional theory to explore relationships between microscopic forces and equilibrium configurations of grafted nanoparticles. Chremos et al.[37,38] performed coarse-grained molecular dynamics simulations to generate morphology maps as a function of particle size, grafting density, and temperature and investigated NOHMs dynamics.[39] Extensive oscillatory and shear rheological measurements have been obtained experimentally for different NOHMs systems,[13,14,40] but there are no comparable simulation studies except for Goyal and Escobedo's coarse-grained simulations of NOHMs recently which reported shear-thinning effects and analyzed the cause at the molecular scale.[41] The present study addresses further this gap by focusing on calculations of the transport properties, in particular focusing on the viscosity and diffusivity. No prior

Received: November 22, 2011
Revised: January 13, 2012
Published: January 13, 2012

   dx.doi.org/10.1021/jp2112582 | J. Phys. Chem. B 2012, 116, 2385−2395

Table 1. Systems Investigated

system	description	particle diameter (nm)	no. particles in system	no. chains in system	grafting density (nm^{-2})
SE_{12}	POSS particle + 8 grafted dodecamers	0.902	60 and 120	480 and 960	3.13
LE_{12}	SiO_2 particle + 12 grafted dodecamers	2.0	80	960	0.95
LE_6	SiO_2 particle + 12 grafted hexamers	2.0	130	1560	0.95
L/E_{12}	SiO_2 particle + free dodecamers	2.0	80	960	
L/E_6	SiO_2 particle + free hexamer	2.0	130	1560	
E_{12}	bulk dodecamer			100	
E_6	bulk hexamer			150	

studies of viscosity have been performed in atomistic models for grafted or ungrafted nanoparticles in a medium of chains.

Deviations from the Stokes–Einstein relation have been observed for supercooled liquids,[42,43] charged molecules,[44,45] and low molecular-weight diffusants.[46,47] In nanocomposites, a breakdown of the Stokes–Einstein relation has been predicted[48−51] when particle size is comparable to that of polymer molecules through which they diffuse, because of "segmental friction" the particles experience, different from the friction of continuum bulk solvents the Stokes–Einstein relation assumes. This prediction was confirmed by both experiments and simulations.[35,52] On the other hand, simulations are also available that confirm the Stokes–Einstein relation holds at an atomistic scale and can be used to estimate the particle sizes in simple liquids.[53,54] Thus, it is of interest to examine the validity of the Stokes–Einstein relation in NOHMs systems.

Although both viscosity and diffusivity are easy to calculate in coarse-grained models, it is hard to match the results quantitatively with experiments. Models with atomistic descriptions of both nanoparticles and oligomers have not been used to study dynamic processes slower than the end-to-end distance relaxation of chains (~2.5 ns).[26] In the present work, we use a model with a reduced number of interaction sites for the silica nanoparticles but keep an atomistically detailed description for the poly(ethylene oxide) (abbreviated as "PEO" from here on) oligomer chains. The coarse-grained representation of nanoparticles reduces the number of interaction sites by a large factor (e.g., 200 for a 2 nm-diameter particle of mass density ρ = 1.8 g/cm^3).[55] Even then, our studies have to be performed at temperatures above 500 K so that diffusive behavior of cores can be observed within computationally affordable time-scales on the order of 100 ns. Experimentally, thermal decomposition of PEO starts at ~400 K,[56] so extrapolation in temperature is necessary for comparisons to experimental data. A similar strategy was used by Ndoro et al,[21] who studied the equilibrium structure of atomistic particle polystyrene nanocomposites, with simulation temperature set to be 590 K, above the thermal decomposition temperature of polystyrene around 400−500 K.[57] We explore the temperature dependence of viscosities and diffusivities and extrapolate the computed transport properties down to experimentally accessible temperatures. In addition to the core distributions and diffusion coefficients, chain and subchain dynamics at different length scales are analyzed through the Rouse modes,[58] which can provide insights into the contrast between NOHMs' liquidlike rheology and nanocomposites' solidlike behavior.

The remainder of this paper is organized as follows. In section 2, we present the model and simulation details. Section 3 discusses the results, including property predictions, temperature dependence of viscosity and diffusivity, analysis of the Stokes–Einstein relation, and chain dynamics. Conclusions are summarized in section 4.

2. MODELS

2.1. Potentials. This work focuses on bulk systems of silica particles grafted by $-O(CH_2CH_2O)_nCH_3$ oligomer chains and free SiO_2 particles immersed in $CH_3O(CH_2CH_2O)_nCH_3$ chains. Two different sizes were chosen for particles, in particular diameters d = 2 nm and d = 0.902 nm. Computational limitations make it difficult to investigate particles larger than 2 nm and atomistic chains, although the diameters of silica particles in experiments vary between 8 and 20 nm.[6,7,13,14,40,55] The smaller particles (d = 0.902 nm) represent polyhedral oligomeric silsesquioxanes (POSS) cages, which are an excellent possible substitute for SiO_2 cores, due to the increased fluidity of the resulting composites.[40] For simplicity, the short bridges (usually organosilane[13,14]) which attach PEO oligomers to nanoparticles were omitted in the model. We considered two chain lengths − hexamers (n = 6) and dodecamers (n = 12), and studied both grafted particles with no solvent (NOHMs) and ungrafted particles in a medium of chains (nanocomposite) systems. Table 1 summarizes the sizes and other parameters in different systems and list the acronyms used to refer to each system in the following sections.

We use solid spheres instead of atomistically described SiO_2 or POSS particles but keep the atomistic representation for grafted PEO oligomers, which form major parts of the grafted chains of many experimentally synthesized NOHMs.[13,14,40] Similarly, in the nanocomposite systems, free silica particles are coarse-grained into one solid sphere, and the free PEO chains are treated atomistically. The SiO_2 chemistry is preserved by setting the particle−particle potentials to be the integration of all pairwise potentials between Si and O atoms from the two particles and similarly particle−atom potentials the summation of all Si/O-X (X = CH_3, CH_2, O in oligomers) potentials in one particle, in the assumptions of additive van de Waals interactions based on London theory.[59] In particular, the interparticle potential is calculated by

$$U_{pp}(r) = \sum_{\alpha,\beta=Si,O} \rho_{1,\alpha}\rho_{2,\beta} \int_{V_1}\int_{V_2} U_{\alpha\beta}(r_{12})\, dV_1\, dV_2 \quad (1)$$

where r is the distance between the two particles, r_{12} is the interatom distance, and ρ_α is the number density of atom α (α = Si, O) in one particle. For interparticle potentials following the Lennard-Jones (LJ) form

$$U(r_{12}) = 4\varepsilon\left[\left(\frac{\sigma}{r_{12}}\right)^{12} - \left(\frac{\sigma}{r_{12}}\right)^{6}\right] \quad (2)$$

dx.doi.org/10.1021/jp2112582 | J. Phys. Chem. B 2012, 116, 2385−2395

integration of the attractive part and the repulsive terms over two single-atom-type spheres has been obtained by Hamaker[60] and Everaers and Ejtehadi,[61] respectively. In addition to the flexibility it affords for density adjustment of the nanoparticles, the integrated LJ potential was found to generate better results around the critical points of bulk nanoparticles than the atomistic representations.[62] This is because the integrated LJ potentials have cutoff radius longer than particle size and do not accumulate errors on length scales smaller than the particle diameter.

For particles including two types of atoms, the integrals give

$$U(r) = -\frac{A_{pp}}{6}\left[\frac{2R^2}{r^2-4R^2} + \frac{2R^2}{r^2} + \ln\left(\frac{r^2-4R^2}{r^2}\right)\right] + \frac{A_{pp}}{37800}\frac{\sigma_{pp}^6}{r}\left[\frac{r^2-14rR+54R^2}{(r-2R)^7} + \frac{r^2+14rR+54R^2}{(r+2R)^7} - \frac{2r^2-60R^2}{r^7}\right] \quad (3)$$

where R is the radius of particles and the coefficients, A_{pp} and σ_{pp} satisfy

$$A_{pp} = 4\pi^2\rho_{Si}(\varepsilon_{Si-Si}\sigma_{Si-Si}^6\rho_{Si} + \varepsilon_{Si-O}\sigma_{Si-O}^6\rho_O) + 4\pi^2\rho_O(\varepsilon_{Si-O}\sigma_{Si-O}^6\rho_{Si} + \varepsilon_{O-O}\sigma_{O-O}^6\rho_O) \quad (4)$$

$$A_{pp}\sigma_{pp}^6 = 4\pi^2\rho_{Si}(\varepsilon_{Si-Si}\sigma_{Si-Si}^{12}\rho_{Si} + \varepsilon_{Si-O}\sigma_{Si-O}^{12}\rho_O) + 4\pi^2\rho_O(\varepsilon_{Si-O}\sigma_{Si-O}^{12}\rho_{Si} + \varepsilon_{O-O}\sigma_{O-O}^{12}\rho_O) \quad (5)$$

Here, σ and ε are diameters and well depths of LJ potentials for Si and O in amorphous silica, $\sigma_{Si-Si} = 0$, $\sigma_{O-O} = 0.299$ nm, $\sigma_{Si-O} = 0.153$ nm, $\varepsilon_{Si-Si} = 0$, $\varepsilon_{O-O}/k_B = 237.8$ K, $\varepsilon_{Si-O}/k_B = 13280$ K, reparameterized by Barbier et al[26] from the Buckingham potential form. Assuming density of the silica particles is 1.80 g/cm^3, the number densities for Si and O can be calculated to be $\rho_{Si} = 18.0$ nm^{-3}, $\rho_O = 36.1$ nm^{-3}. Plugging them into eqs 4 and 5 leads to $A_{pp}/k_B = 17490$ K, $\sigma_{pp} = 0.267$ nm. The cutoff radius of the particle−particle integrated interaction is set as $2.5d$, where d is the particle diameter. Figure 1 compares the integrated LJ potential between particles and between particles and united-atom groups with the LJ potential for O−CH$_3$ interactions. The integrated potetnials have much steeper repulsion at short separations and a deeper attraction well than the LJ potential between two atoms. Particle−particle attractions are 4−12 times greater than the thermal energy at room temperature, respectively, for 1 and 2 nm particles.

For the chains, we use the modified TraPPE-UA force field that has been tested for viscosity and diffusivity calculations of PEO oligomers.[63,64] We further modified the form of the bond potentials and reparameterized the dihedral potentials to use the force field with the LAMMPS package.[65,66] Here, we briefly summarize the TraPPE potential parameters used. Each free chain consists of 3 types of united atoms, CH$_3$, CH$_2$, and O (denoted as "eO" to be distinguished from O atoms in silica), carrying partial charges 0.25 e, 0.25 e, −0.5 e, respectively, on the atom centers. Grafted chains in NOHMs lack one CH$_3$ end, so to keep the system charge-neutral; the oxygen atom attached to the surface in each grafted chain (labeled "fO") is assigned a partial charge of −0.25 e. Except for the partial charge, other parameters of fO atoms are the same as for eO. Nonbonded interactions between

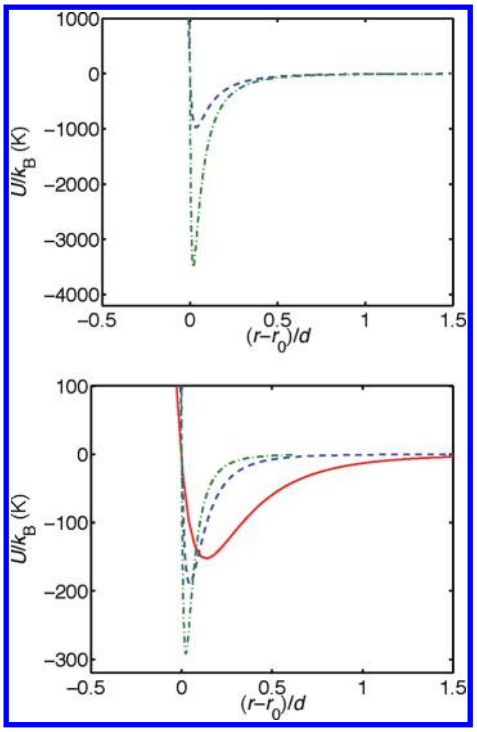

Figure 1. Potentials for particle−particle (top) and particle−atom interactions (bottom). Note the difference in vertical scales. r_0 is the separation at which $U(r) = 0$. Top part, dashed line, 1-nm diameter particle, $d = 1$ nm; dash-dotted line, 2 nm-diameter particle, $d = 2$ nm. Bottom part, solid line is for O−CH$_3$ interactions, $d = \sigma_{O-O}$; the other lines are for particle-CH$_3$ interactions; dashed line, $d = 1$ nm; dash-dotted line, $d = 2$ nm.

the united atoms include pairwise LJ and Coulombic potentials, both truncated at 0.9 nm. The diameters and well depths of the LJ potentials are $\sigma_{eO-eO} = \sigma_{fO-fO} = 0.28$ nm, $\sigma_{CH_2-CH_2} = 0.395$ nm, $\sigma_{CH_3-CH_3} = 0.375$ nm, $\varepsilon_{eO-eO,fO-fO}/k_B = 55.0$ K, $\varepsilon_{CH_2-CH_2}/k_B = 46.12$ K, $\varepsilon_{CH_3-CH_3}/k_B = 98.0$ K. The cross-terms were obtained by using Lorentz−Berthelot combination rules. van der Waals and electrostatic interactions for atoms separated by 3 bonds ("1−4" interactions) were reduced to half of the original strength.

Nonbonded interactions between particles and chain united-atom groups are given by the integrated LJ potential

$$U_{pa}(r) = \sum_{\alpha=Si,O}\rho_\alpha\int_V U_{\alpha-X}(r_{\alpha-X})\,dV \quad (X = CH_3, CH_2, eO, fO) \quad (6)$$

$U_{\alpha-X}$ is the LJ potential between an α atom in the particle and a united atom X in the chains. The integration of eq 6 involving particles with multiple types of atoms have the same analytical form as that for particles consisting of just single type of atoms[66]

$$U_{pa}(r) = \frac{2R^3\sigma_{pa}^3A_{pa}}{9(R^2-r^2)^3}\times\left[1 - \frac{(5R^6+45R^4r^2+63R^2r^4+15r^6)\sigma_{pa}^6}{15(R-r)^6(R+r)^6}\right] \quad (7)$$

with parameters A_{pa} and σ_{pa} for silica particles given by

$$A_{pa}\sigma_{pa}^3 = 24\pi(\varepsilon_{Si-X}\sigma_{Si-X}^6\rho_{Si} + \varepsilon_{O-X}\sigma_{O-X}^6\rho_O) \quad (8)$$

dx.doi.org/10.1021/jp2112582 | J. Phys. Chem. B 2012, 116, 2385−2395

$$A_{pa}\sigma_{pa}^{9} = 24\pi(\varepsilon_{Si-X}\sigma_{Si-X}^{12}\rho_{Si} + \varepsilon_{O-X}\sigma_{O-X}^{12}\rho_{O}) \quad (9)$$

The cross-term LJ parameters in eqs 8 and 9 obey the Lorentz−Berthelot rules except for $\sigma_{Si-eO,fO}$ = 0.153 nm, σ_{Si-CH_2} = 0, σ_{Si-CH_3} = 0, $\varepsilon_{Si-eO,fO}/k_B$ = 13280 K.[26] The bottom panel in Figure 1 compares particle−atom and atom−atom potentials. Both repulsions and attractions of particle−atom potentials are less steep than particle−particle interactions (top panel). Particle−atom attractions are similar in magnitude to the thermal energy.

The SHAKE bonds in modified TraPPE force field were replaced by FENE bonds (eq 10) for use with LAMMPS

$$U_b(r) = \begin{cases} -0.5KR_0^2 \ln\left[1-\left(\frac{r}{R_0}\right)^2\right] + 4\varepsilon\left[(\sigma/r)^{12} - (\sigma/r)^6\right] + \varepsilon & \left(0 < r < 2^{1/6}\sigma\right) \\ -0.5KR_0^2 \ln\left[1-\left(\frac{r}{R_0}\right)^2\right] & \left(2^{1/6}\sigma < r < R_0\right) \end{cases} \quad (10)$$

The bonds are not allowed to extend beyond R_0. We do not use the simpler harmonic bonds because they can result in sampling unphysically large separations given a long enough time[67] (even with large force constants) and consequently change the dynamics. FENE bonds, although less constraining than rigid bonds, generate viscosities within 10% of those of molecules connected by rigid bonds.[68] In one of our test runs with dimethoxylethane at 303.15 K, 1 MPa, the use of harmonic bonds failed to reproduce the viscosity of the same molecule described using rigid bonds in ref 64, while the same molecule with FENE bonds was found to have a viscosity within the error bars of the rigid-bond calculations. In eq 10, we set R_0 = 0.18 nm, σ = 0.147 nm for CH_x−CH_y bonds and R_0 = 0.16 nm, σ = 0.134 nm for CH_x−eO/fO. K = 83680 kJ/(mol·nm^2) and ε = 836.8 kJ/mol for both bonds. The bond potentials with these parameters have minima at 0.154 nm for CH_x−CH_y and 0.141 nm for CH_x−eO/fO, the same as the fixed bond lengths used in modified TraPPE-UA. Densities were examined at 303 K, 0.1 and 1 MPa, with <0.6% differences from that of rigid-bond dimethoxylethane.[64] Rigid-bond PEO oligomers have been shown to reproduce experimental volumetric properties with 1 to 2% discrepancies.[64] Figure 2 shows FENE bonds overestimate the specific volumes of simulated E_6 by 6% at room temperature compared with experiments. As chains further increase to dodecamers, the agreement becomes better (1% difference).

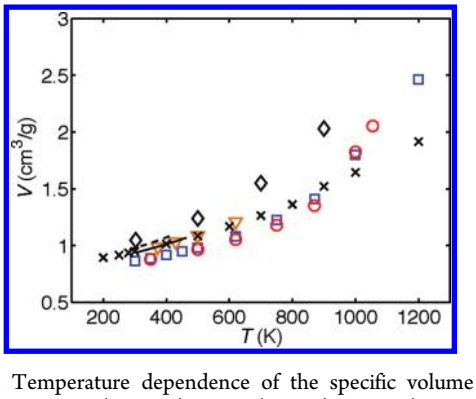

Figure 2. Temperature dependence of the specific volume at zero pressure for LE_{12} (squares), LE_6 (circles), SE_{12} (triangles), E_{12} (crosses), E_6 (diamonds), and experimental data of pentamers (n = 5)[73] at 10 bar (dashed line) and PEODME ($M \approx 600$)[74] at 0 bar (solid line).

In NOHMs, the first oxygens (fOs) together with the central particle are treated as a rigid body, translating and rotating as one entity. The distance between fO and the particle surface is fixed to be 0.16 nm ($\sim\sigma_{Si-fO}$). For both grafted and ungrafted PEO oligomers, the bond angle potentials have the original TraPPE-UA harmonic form and parameters, $U_\theta = k_\theta(\theta - \theta_0)^2$. The force constants, k_θ, and the equilibrium angles, θ_0, remain the same as in TraPPE,[63,67] k_θ = 251.1 kJ/(mol·rad^2), θ_0 = 112° for particle CH_x-eO/fO−CH_y and k_θ = 209.1 kJ/(mol·rad^2), θ_0 = 112° for eO/fO−CH_x-eO/fO. Fischer et al[63] modified the TraPPE dihedrals for PEO, which generate volumetric data in better agreement with experiments. Here we adopted Fischer's dihedrals but fit them using a LAMMPS functional form, $U_d(\phi) = \Sigma_{n=1}^{5} A_n \cos^{n-1}(\phi)$. The parameters were obtained as, A_1/k_B = 193.5 K, A_2/k_B = −2551 K, A_3/k_B = −940 K, A_4/k_B = 2574 K, A_5/k_B = 773 K for particle CH_x−eO/fO−CH_y−CH_z and A_1/k_B = 267 K, A_2/k_B = −2119 K, A_3/k_B = 1004 K, A_4/k_B = 4041 K, A_5/k_B = 608 K for eO/fO−CH_x−CH_y−eO/fO.

2.2. Simulation Details. We used the following procedure to obtain states for NOHMs corresponding to atmospheric pressure, which for simulations of condensed phases can be considered equal to zero. Oligomer-grafted particles were first placed randomly in a box of large volume. We temporarily replaced the rigid particle−fO connections with a harmonic bond (force constant k_0 = 209200 kJ·mol^{-1}·nm^{-2}, equilibrium length r_0 = 1.16 nm) and set σ_{fO-fO} = 0.78 nm to prevent the attached oxygens from aggregating on the particle surface, and performed constant-pressure (*NPT*) simulations to compress the box. The rigid-body treatment of the central particle with its attached fOs was then restored, and *NVT* simulations at several volumes performed until the pressure was near zero. This procedure is necessary because there are no barostats for systems with rigid bodies in LAMMPS. The volumes of nanocomposites were set to be the same as those of NOHMs at the corresponding temperatures, so that grafted and ungrafted systems have the same core volume fractions. For bulk oligomers, we performed simulations in the *NPT* ensemble to obtain an equilibrium volume, at which *NVT* runs were subsequently conducted. The time step was 0.5 fs for particle-containing systems and 0.75 fs for oligomers; these relatively small values are necessary because of the fast bond vibrations introduced by the FENE bonds. Equilibration periods were 8−40 ns and production periods 50−80 ns, depending on temperature, which ranged from 1200 to 500 K. Shorter runs were used at higher temperatures. Bulk oligomers equilibrate faster, so equilibration and production periods were shortened to 3 and 15 ns, respectively.

Table 1 lists the number of particles and chains for all systems studied. The number of particles was such that the systems were small enough to be simulated within the available computing resources but large enough to avoid particles interacting with their periodic images. With the chosen particle and chain numbers, each large silica nanoparticle of NOHMs is grafted with 12 chains and each POSS particle 8 chains. The grafting densities (Table 1) fall within the typical experimental range, from 0.9 to 5 chains nm^2.[13,40,55,70] The number of interaction sites of the large systems is approximately 3 × 10^4, which requires ~15 CPU days to complete 50 ns of simulation, when running in parallel on 24 Intel Xeon X5650 2.67 GHz cores.

2.3. Methods. We applied the Green−Kubo formalism to calculate the viscosity[71]

$$\eta = \frac{V}{k_B T}\int_0^\infty \langle P_{\alpha\beta}(t + t_0)P_{\alpha\beta}(t_0)\rangle \, dt \quad (11)$$

dx.doi.org/10.1021/jp2112582 | J. Phys. Chem. B 2012, 116, 2385−2395

$P_{\alpha\beta}$ is the off-diagonal element in the pressure tensor. Only one prior study employed this method for a coarse-grained model of nanocomposites.[34] The advantage of the Green−Kubo approach over nonequilibrium alternatives is that it is free from the external perturbations that may modify the structure and impose alignment nanoparticle systems. The Green−Kubo method obtains dynamics for equilibrium structures, allowing identification of the structural cause of any dynamical anomalies. We had previously applied this method to compute the viscosity of bulk atomistic PEO oligomers at room temperature.[64] Because of the fast bond vibrations of the present model, output of $P_{\alpha\beta}$ was every 2 time steps in order to capture the fluctuating features of its autocorrelation function. Diffusion coefficients were obtained from the slopes of the mean square displacements (MSD)

$$D = \frac{1}{6}\lim_{t\to\infty}\frac{\mathrm{d}}{\mathrm{d}t}\langle[\mathbf{r}_i(t+t_0) - \mathbf{r}_i(t_0)]\rangle \tag{12}$$

where $\mathbf{r}_i(t)$ is the position of the center-of-mass of the ith particle. The statistical errors given in section 3 are for 95% confidence limits. They were obtained by dividing the time origins in eqs 11 and 12 into 10 and 5 blocks, respectively. More details of viscosity and diffusivity calculations and the estimation of errors can be found in ref 64.

The effects of grafting on oligomer chains dynamics were analyzed through the relaxation of Rouse modes, $\mathbf{X}_p(t)$

$$C_p(t) = \langle \mathbf{X}_p(t)\cdot\mathbf{X}_p(0)\rangle/\langle \mathbf{X}_p(0)\cdot\mathbf{X}_p(0)\rangle \tag{13}$$

This relationship allows us to examine the chain motions from the length scale of the entire chain down to segmental length scale.[58] The Rouse modes are defined as

$$\mathbf{X}_p(t) = \left(\frac{2}{N}\right)^{1/2}\sum_{i=1}^{N}\mathbf{r}_i\cos\left[\frac{p\pi}{N}(i-1/2)\right]$$
$$(p = 1, ..., N-1) \tag{14}$$

These represent the local motions of the chain subsection which includes N/p segments, with N the number of segments per chain, and $\mathbf{r}_i(t)$ the position of the center-of-mass of the ith segment in the chain at time t. We choose the triplet of CH_x−eO/fO−CH_y to be one segment. In NOHMs, the eliminated CH_3 in the first triplet is substituted by the surface position where fO is connected. We found that down to the length scale of two triplets there are no observable differences in the correlation function decays between grouping a triplet into a segment and just taking one atom as a segment for the pure dodecamer (E_{12}) chain system at 500 K.

3. RESULTS AND DISCUSSION

3.1. Volumetric Properties. The specific volumes of NOHMs and oligomer bulks are given in Figure 2 as a function of temperature. We have pointed out in section 2.1 that the introduction of FENE bonds increases the error for volumetric properties of E_6 at room temperature to about 6%. However, the modified force field still predicts the specific volumes of E_{12} very well. Figure 2 shows there is a change in the slope of the specific volume vs temperature for bulk E_6 around 600 K, which coincides with the experimental boiling point, ∼632 K, of hexamers.[72] The simulated E_6 systems above 600 K are therefore superheated liquids. Although E_6 and E_{12} exhibit different compressibilities, LE_{12} and LE_6 have very close specific volumes and expand in a similar fashion. The expansions of both accelerate when the temperature rises to around 800 K. This indicates the dominant roles of nanoparticles and the grafted chain lengths have little effect on the volumetric properties. Experiments have reported that PEO with molar mass of 4000 g/mol exhibits a glass transition at 206 K.[75] We thus expect that the glass transition temperature T_g for hexamers and dodecamers (molar mass ∼600 g/mol) is below 200 K. MSD data discussed in section 3.3 show that both grafted and free particles are diffusive (over simulation time scales) down to 500 K. This indicates that the change in slope seen around 800 K for the grafted nanoparticle systems is not related to the glass transition. This is consistent with prior experiments and simulations of related systems: Brown[17] reported $T_g \approx 250$ K for simulated nanocomposites (silica particles in free n-alkanes). Silica particles ionically grafted by 3-armed PEO amines (molar mass ∼1500 g/mol) were found to have T_g at ∼220 K experimentally.[70] Thus the temperature ranges in which we computed the transport and dynamic properties and to which we extrapolate the data are above any glass transitions for all systems under study.

We estimated the average closest distance between the surfaces of two particles, r_c, via the relationship $r_c = (V/N_p)^{1/3} - d$, where N_p is the number of particles. The closest distance r_c rises from 0.63 to 1.23 nm from 500 to 1000 K for LE_{12}, surpassing the root-mean-square radius of gyration of dodecamers in E_{12} (∼0.77 nm) around 700 K. Similarly, for LE_6, r_c increases from 0.35 to 0.90 nm in the temperature interval 500−1000 K. R_g in corresponding bulk hexamers is calculated to be ∼0.51 nm, surpassed by r_c around 700 K as well. Thus, the volume expansion acceleration of LE_{12} and LE_6 around 800 K could be attributed to structural changes of the grafted oligomers. Below this temperature, the influence of the grafting topology, which extends the oligomers, is balanced by the confinement due to close interparticle distances of the oligomers. At temperatures above 800 K in which $r_c > R_g$, the confinement effects diminish and chains stretch. The stretching configurations result in an additional repulsive entropic force between two layers of opposing polymer brushes[76] and accelerate temperature expansion. Similar trends, although not obvious, can be observed from the root-mean-square end-to-end distances, r_{ee}, of oligomers. From 500 to 1000 K, r_{ee} increases from 2.0 to 2.05 nm for grafted dodecamers, 1.36 to 1.37 nm for grafted hexamers. In the same temperature range, r_{ee}s decrease from 2.03 to 1.97 nm and 1.38 to 1.36 nm for E_{12} and E_6, respectively, as temperature rises. There are rough crossovers between grafted and bulk oligomers of the investigated chain lengths, showing the grafted chains at low temperatures behave more bulklike.

Particle−particle radial distribution functions $g_{pp}(r)$ at 500 K for LE_{12}, LE_6, and its ungrafted analog, L/E_{12}, L/E_6 are given in the top panel of Figure 3. Both have a high first peak at ∼2.15 nm, corresponding to a bond-length separation between the closest points within particle pairs. This shows that there is significant particle aggregation, especially for the nanocomposite systems that do not have a grafted oligomer layer. The inset is a zoomed-in plot for those low peaks at $r > 2.2$ nm. More ordered structures can be observed in nanocomposites while NOHMs exhibit liquidlike long-range distributions. For the nanocomposite systems, we also observed that the first peak heights, averaged over different stages of the production period, kept changing. The bottom panel of Figure 3 presents the fluctuation range of the first peak heights, for NOHMs and

dx.doi.org/10.1021/jp2112582 | J. Phys. Chem. B 2012, 116, 2385−2395

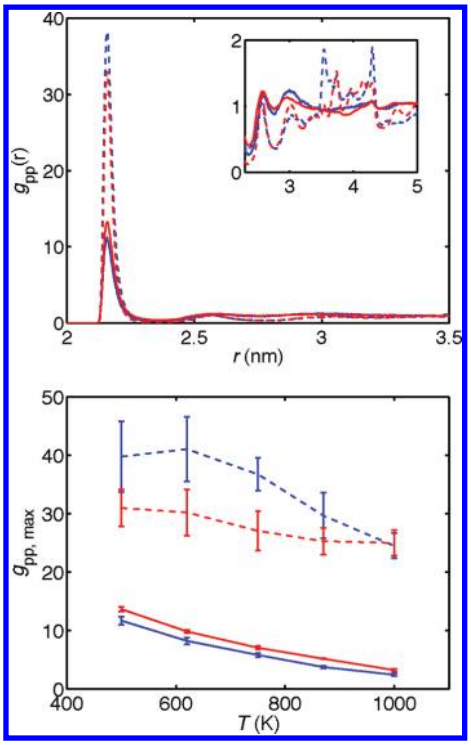

Figure 3. Particle−particle radial distribution functions at 500 K as a function of distance (top) and its maximum value as a function of temperature (bottom). LE_{12} (blue solid line) and L/E_{12} (blue dashed line), LE_6 (red solid line), L/E_6 (red dashed line). The inset in the top figure is a zoomed-in plot for low peaks at $r > 2.2$ nm.

nanocomposites, over the temperature range 500−1000 K. Particles in LE_6 have slightly more close contacts (higher $g_{pp,max}$) than those in LE_{12} due to the thinner surrounding oligomer layers formed by the shorter hexamers. By contrast, in nanocomposites, particles immersed in short chains (L/E_6) are surrounded by fewer neighbor particles relative to the same systems with longer chains over the entire temperature range of $T < 1000$ K. This is because unattached hexamers have a higher mobility than dodecamers and therefore have a higher probability to squeeze into the interparticle region.

Chremos et al.[37] have obtained structural "maps" of grafted nanoparticle (NOHMs) systems, identifying regions where aggregates, glasses, and liquid structures occur, as functions of grafting density, oligomer length, and particle size. To make a connection with that study, we group CH_x−eO/fO−CH_y into one bead, resulting in a coarse-grained bead size of σ_b = 0.42 nm—the distance at which the coarse-grained nonbonded potential between coarse-grained beads is zero.[77] Then, the reduced particle diameter in LE_{12} and LE_6 can be calculated to be $4.8\sigma_b$. From 1000 to 500 K, the reduced oligomer matrix densities, ρ_b, range from 0.40 to 0.82 for LE_{12} and from 0.30 to 0.71 for LE_6. The LE_{12} and LE_6 systems in Figure 3 thus all lie in the liquid region of the f-ρ_b map of Figure 3 in ref 37 with the two T = 500 K systems roughly on the liquid−aggregation border. Figure 4 shows a good dispersion of particles in NOHMs at 500 K. But the first peaks of $g_{pp}(r)$ in this work are as high as those for aggregated systems in Figure 1 of ref 27. This difference may be caused by different resolution (coarse-grained vs atomistic) of the two studies. Coarse-grained beads have larger excluded volumes than the atomistic segments they are representing. For nanocomposites in Figure 3, the extremely high first peaks of g_{pp} indicate formation of gel-like

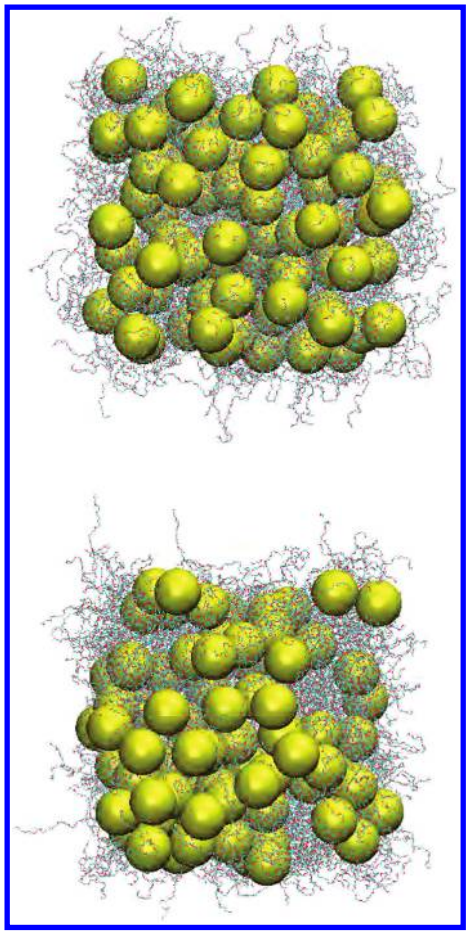

Figure 4. Snapshots of LE_{12} (top) and L/E_{12} (bottom) at 500 K. Yellow spheres represent the silica nanoparticles, cyan lines are CH_3 and CH_2 united atoms and red lines represent oxygens.

structures. Prior studies[7,78] indicate that the percolation thresholds for nanocomposites can be as low as 10 vol % of particles, if there are attractive interactions of range comparable to particle size. In our work, the volume fraction of particles ranges between 12 and 23% for L/E_{12} and 17−32% for L/E_6 from 1000 to 500 K, suggesting a high likelihood of network formation. Typical snapshots of our systems are shown in Figure 4. The bottom panel (nanocomposites) clearly shows more aggregations of particles and more space void of particles exist in L/E_{12} that in LE_{12} at 500 K. However, the particles in nanocomposites become diffusive eventually, as indicated by the MSD data in section 3.3. The particles are not permanently trapped in the aggregates, so we still calculate the viscosities and diffusivities for ungrafted systems.

3.2. Viscosities. We plot viscosities as functions of temperature for nanocomposite and bulk oligomer systems in Figure 5 and for NOHMs systems in Figure 6. The simulations cannot give values of viscosities at lower temperatures for NOHMs systems, because reaching the relevant time scales is impractical. Instead, viscosities are obtained via extrapolation from higher temperatures for which computations are feasible. In section 3.1, we have established that all simulated systems are at temperatures above their respective T_gs. By assumption that no other transitions take place, viscosity is expected to depend on T with an Arrhenius behavior,[79,80] $\eta = \eta_0 \exp(E/RT)$. We first check whether the extrapolation method gives consistent results by examining bulk oligomers for which the

dx.doi.org/10.1021/jp2112582 | J. Phys. Chem. B 2012, 116, 2385−2395

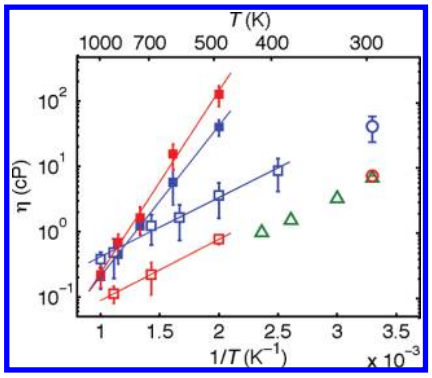

Figure 5. Temperature dependence of viscosities for nanocomposite and free chain systems. L/E_{12} (filled blue square), L/E_6 (filled red square), E_{12} (hollow blue square), E_6 (hollow red square), E_{12} with rigid bonds[64] (hollow blue circle), E_6 with rigid bonds[64] (hollow red circle), and experimental data[73] (green triangles). Lines are linear-least-squares fits to the corresponding data.

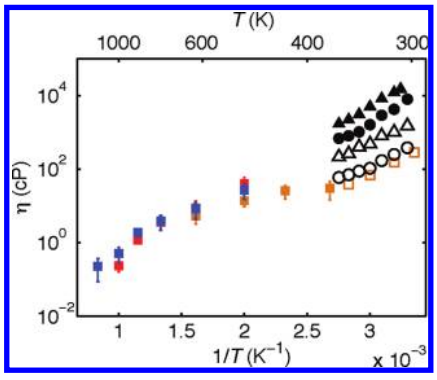

Figure 6. Temperature dependence of viscosities for NOHMs systems. SE_{12} (filled orange squares), LE_{12} (filled blue squares), LE_6 (filled red squares). Experimental data from ref 81 for POSS-$CH_2CH_2(OCH_2CH_2)_mOCH_3$, $m \approx 13.3$ (hollow orange square), and from ref 40 for POSS-NOHM-C-HPE with 10 w% (hollow circle) and 30 w% (filled circle) of cores, particle-NOHM-C-HPE (silica particle, 10 to 15 nm diameter) with 15 wt % (hollow triangle) and 30 wt % (filled triangle) of cores.

viscosities around room temperature are already available.[64] Figure 5 shows the temperature dependence of viscosities for E_{12} and E_6 at temperatures from 400 to 1000 K. Extrapolation using the Arrhenius equation for E_{12} leads to a viscosity within the error bar of that obtained directly by the Green–Kubo method, 41 ± 17 cP, at 303 K. The extrapolated viscosity of E_6 is around 80% higher than the interpolated value from direct calculations of pentamers and nonamers at 303 K. Figure 5 also includes the experimental data for hexamers, which have the similar slope as that of E_6. It indicates simulations capture the activation energy of hexamers in experiments.

Viscosities for simulated and experimental NOHMs systems are presented in Figure 6. The data points of SE_{12} have a smaller slope than the experimental data, but overlap with them around room temperature. For LE_{12} and LE_6, gradual changes of slope are observed around 800 K. In section 3.1, we pointed out there are chain configurational changes around 800 K in LE_{12} and LE_6, leading to higher thermal expansion coefficients. Together with the trend reflected by $g_{pp,max}$ in Figure 3 that aggregation increases as T drops, the different slopes suggest that structural transitions take place in NOHMs over the range of temperatures studied. Although it is still far from T_g, a soft glass structure has been proposed for grafted nanoparticles around room temperature.[13,82] Experimental data in Figure 6 have slightly different slopes at low and high temperatures. "Super-Arrhenius" expressions, e.g., the empirical Vogel–Fulcher–Tamman (VFT) equation $\eta = \eta_0 \exp[T_0/T - T_0)]$[83] or the power law $\eta = \eta_0 \exp(T/T_x - 1)^a$ suggested by theories,[43,84] may be necessary to describe the viscosities at low temperatures.

For both nanocomposites (Figure 5) and NOHMs (Figure 6), systems with longer chains have smaller viscosities than those with shorter chains at lower temperatures, but the opposite is true at high temperatures. These observations are determined by two competing factors: volume fraction of particles and chain entanglement. Volume fraction is important at low temperatures where the chains are confined and hardly have relative motions over the chain length scale. Longer chains occupy the more space, reduce the fraction of hard particles and consequently decrease the "hardness" of the systems. At high temperatures, the interparticle space is greatly increased and chains can move freely or are carried over distance larger than the chain size, so chain entanglements become dominant. Experiments generally graft particles with chains of the lengths in the "polymer" range. With significantly increased organic content, the volume fractions of particles and their effects are small even if it is at low temperature. In such systems, we expect the motion of particles are no longer confined by neighbor particles and the first trend above that NOHM with longer chains have lower viscosities may not be observed. From the viscosity-temperature curves shown in Figures 5 and 6, we find that ungrafted (nanocomposite) systems have larger slopes (or "activation energies") than NOHMs. These higher-energy barriers in nanocomposites may be attributed to stronger aggregation and suggest that the viscosity increases much less rapidly at lower temperatures for NOHMS relative to nanocomposites; thus, it may explain the fluidlike behavior of many NOHMs systems at room temperature. As mentioned in the introduction, experiments used short chains for NOHMs but longer chains for nanocomposites. Since grafted systems and ungrafted systems here have the same chain length, our work excludes the chain length difference as a possible explanation for the cause to NOHMs' higher fluidity.

3.3. Diffusivities. Before reporting diffusivities, mean square displacements (MSDs) of NOHMs and nanocomposites need to be examined in order to ensure the diffusive regimes are reached. Figure 7 shows that over the simulation times, at

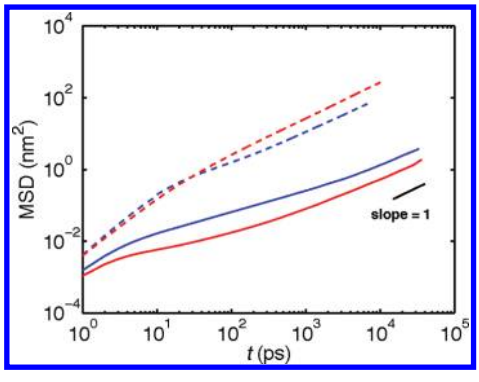

Figure 7. Mean square displacements (MSDs) of LE_{12} (blue) and the particles in L/E_{12} (red) at 500 K (solid line) and 1000 K (dashed line).

dx.doi.org/10.1021/jp2112582 | J. Phys. Chem. B 2012, 116, 2385–2395

low temperatures both grafted and ungrafted particles exhibit a ballistic regime and a subdiffusive regime, before entering the diffusive regime. At high temperatures, the subdiffusive plateau disappears. It has been pointed out in section 3.1 that there are nanoparticle aggregates, especially in nanocomposites, with a high value of the pair correlation function between particles. The MSD data presented here suggest that these aggregates are transient. Surrounding particles block particles in "cages" but do not trap them permanently. Larger aggregates are more effective in delaying particle movement, so free particles diffuse more slowly than grafted particles at low T (T = 500 K, blue continuous line is over the red one in Figure 7). At high T (1000 K), although there are still aggregates forming small clusters ($g_{pp,max} \sim 25$), the average interparticle surface distance $r_c = (V/N_p)^{1/3} - d$ has been expanded to as large as 1 and 1.5 nm for hexamer- and dodecamer-included nanoparticle systems, respectively. The caging effect thus disappears for a free particle, and no subdiffusive plateau is observed for nanocomposites. However, because of the stretched chain configurations, grafted particles carrying a thick layer actually have a larger effective size than free ones and turn out to diffuse more slowly (blue dashed line is under the red one in Figure 7). The influence of grafting on the MSDs at different temperatures is consistent with the observed behavior of the viscosities in (Figure 5). The same effects on the MSDs were reported by Chremos et al.[39] for coarse-grained models of NOHMs.

Diffusion coefficients as the function of temperature are shown in Figure 8 for NOHMs and bulk oligomers. In

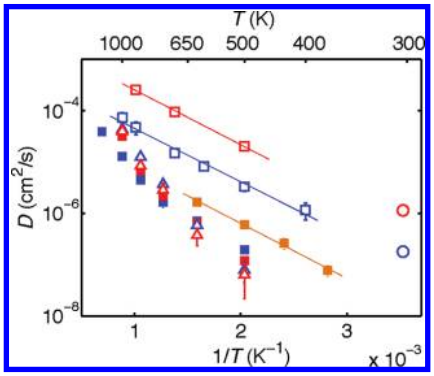

Figure 8. Temperature dependence of diffusivities of NOHMs, nanocomposites, and bulk oligomers: SE_{12} (filled orange square), LE_{12} (filled blue square), LE_6 (filled red square), L/E_{12} (hollow blue triangle), L/E_6 (hollow red triangle), E_{12} (hollow blue square), E_6 (hollow red square). Direct calculations from MSD of rigid-bond dodecamers (hollow blue circle) and rigid-bond hexamers (hollow red circle)[64] are also shown. Lines are linear-least-squares fits to the corresponding data.

agreement with the effect of chain length on viscosities, nanoparticles grafted with shorter chains diffuse faster at high temperatures above 800 K due to fewer entanglements but become slower around 500 K where the larger volume fractions of particles become more important. The diffusion–temperature curves for NOHMs also exhibit a transition around 800 K, coinciding with the volume expansion transition, seen also in the η-T curves. Above 800 K, NOHMs diffuse with stretched chains, while below 800 K chains from different particles mix and entangle with each other in a similar way to the melt oligomers.

Extrapolation of the diffusion coefficients to room temperature by the Arrhenius equation gives the diffusivity of E_{12} at 303 K to be around the half of the direct estimation from MSD slopes, $(0.018 \pm 0.002) \times 10^{-5}$ cm^2 s at that temperature. The diffusivity from MSD result for bulk hexamer is also estimated to be 2–3 times of the extrapolated values of E_6.[64] The comparisons indicate extrapolation generates around 50% precision over the whole simulated temperature range. Some curvature is actually observed in the D-T curve of E_{12} and E_6. We obtain a diffusivity for E_{12} within the error from direct MSD calculations if the extrapolation just uses the points between 400 and 600 K and a diffusivity around 40% smaller than the direct MSD estimation for E_6 if only the two points at 500 and 700 K are utilized for extrapolation. By assumption that no transitions take place from 500 to 300 K, extrapolation of the diffusivities of LE_{12}, LE_6, and SE_{12} gives values at 300 K of 3×10^{-9} cm^2/s, 1×10^{-9} cm^2/s, and 1×10^{-8} cm^2/s, respectively. Thus, around room temperature, chain length has small effects on the diffusivity of NOHMs, but the particle size influences significantly.

Figure 8 also presents the temperature dependence of diffusivities for free particles in nanocomposites. Again we see the opposite effects of grafting at low and high temperatures, the same as for the η-T relation. Grafting enhances the correlation between particles and chains, resulting in higher mobility of grafted particles at low temperatures than free particles. Aggregation is another contributing factor to the slow diffusion of free particles. It is hard to tell which factor, aggregation or correlation, plays a more significant role in the higher fluidity of NOHMs relative to conventional nanocomposites.

3.4. Validity of the Stokes–Einstein Relationship. It has been reported[35,46,47] that if a diffusing particle's size is comparable to the size of the solvent molecules, it experiences a friction caused by solvent molecule segments, different from the macroscopic viscosity, and as a result the Stokes–Einstein relation breaks down. In simulated gold nanoparticles diffusing in liquid argon, the critical size under which Stokes–Einstein relation does not hold is around 0.5 nm.[47] Liu et al[35] tested the Stokes–Einstein relation in nanocomposites and found that deviations occur if $R/R_g < 0.7$ where R and R_g are the particle radius and the radius of gyration of polymers, respectively. Statistical dynamical theory was used by Yamamono and Schweizer,[50] which predicts the critical size is $R = 1.5R_g$ for one particle immersed in free unentangled polymers. The bulk dodecamers in this work has $R_g \approx 0.85$ nm. The R/R_g for our grafted or free particle systems are then estimated to be ~1.2 for 2-nm particles and ~0.53 for POSS, very close to the reported critical size. It is therefore important to examine whether the Stokes–Einstein relation holds to our systems and, if it is not, how grafting affects the critical size.

Figure 9 gives the estimated hydrodynamic radii, R_h, for NOHMs (top) and particles in nanocomposites (bottom) from the Stokes–Einstein relations assuming slip boundary condition

$$R_h = \frac{k_B T}{4\pi\eta D} \tag{15}$$

and stick boundary condition

$$R_h = \frac{k_B T}{6\pi\eta D} \tag{16}$$

dx.doi.org/10.1021/jp2112582 | J. Phys. Chem. B 2012, 116, 2385–2395

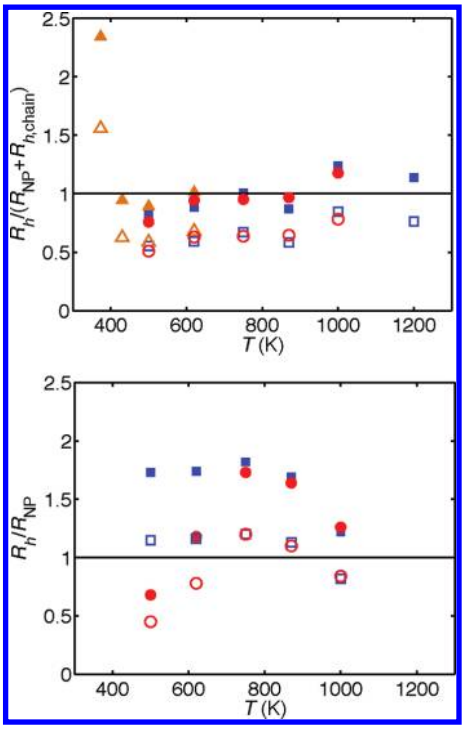

Figure 9. Hydrodynamic radii estimated from the Stokes−Einstein relation in the assumptions of slip (filled) and stick (open) boundary conditions of particles for NOHMs (top) and nanocomposites (bottom). Squares, LE_{12}, L/E_{12}; circles, LE_6, L/E_6; triangles, SE_{12}. The hydrodynamic radius of oligomers, $R_{h\ chain}$, is estimated to be 0.3 nm for E_{12} and 0.24 nm for E_6.

for the nanoparticle surfaces, respectively. Prior studies suggest that the stick boundary condition can only be achieved by atomistic models of nanoparticles with strong particle−atom interactions.[47,85] This agrees with our results of NOHMs using coarse-grained solid-sphere representation for nanoparticles. $R_{h,chain}$ used in Figure 9 are the hydrodynamic radii of the oligomers, estimated by eq 16 to be 0.3 nm for E_{12} and 0.24 nm for E_6. $R_{NP} + R_{h,chain}$ is a rough estimation of the hydrodynamic radius of NOHMs. R_h's obtained by eq 15 are located closely to $R_{NP} + R_{h,chain}$, but R_h's calculated with the assumption of stick boundary condition are even less than the nanoparticle radius, R_{NP}. So stick boundary condition significantly underestimates the true hydrodynamic radius. There is a sudden jump of the R_h for SE_{12} at 373 K. It is considered to be caused by the failure of the Green-Kubo approach because of insufficient sampling, rather than a breakdown of the Stokes−Einstein relation. Deviations from Stokes−Einstein relation caused by proximity to a glass transition is a gradual process as T decreases. However, the R_h's for free particles in the bottom panel of Figure 9 show calculations by eq 16 generate R_h results closer to the radius of particle. Here we think the slip boundary condition should still be used for nanocomposites. This is because particle aggregation exists in nanocomposites. The aggregation raises the R_h's from eq 15, making R_hs deviate from the Stokes−Einstein law. Aggregation also raises the estimated R_h's in eq 16, and happens to canceling the underestimation of eq 16 if there were no aggregation. As a combined result, the stick boundary condition assumption generates R_h close to R_{NP} by accident.

The viscosities we used in eqs 15 and 16 are the viscosities of NOHMs and nanocomposites, rather than the viscosities of bulk oligomers as used in previous literature.[35,47] It can be interpreted as one grafted particle diffusing in the solvent of NOHMs or one free particle moving in nanocomposites solvent. If the viscosities of bulk oligomers are adopted in eqs 15 and 16, the Stokes−Einstein relationship does not hold, because the systems have high particle volume fractions, while the Stokes−Einstein relation was derived in the dilute limit.

3.5. Chain Dynamics. To further understand the roles played by the chains, the relaxation of the correlation function of Rouse modes, $C_p(t)$, defined in eq 14, are computed and plotted in Figure 10 for LE_{12} and L/E_{12} at 500 and 1000 K. For Rouse chains, C_p relaxes following the expression

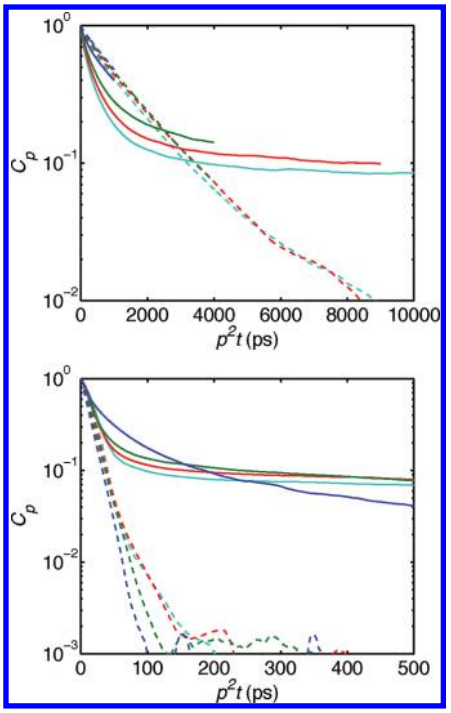

Figure 10. Relaxation of C_p for grafted dodecamers (solid line) in NOHMs and free dodecamers (dash line) in nanocomposites at 500 K (top) and 1000 K (bottom). Blue, $p = 1$; green, $p = 2$; red, $p = 3$; cyan, $p = 4$.

$$C_p = \exp(-t/\tau_p) \qquad (p \geq 1) \tag{17}$$

where the relaxation time of the p-th mode satisfies

$$\tau_p = \tau_1 / p^2 \tag{18}$$

The overlaps for the C_p-t curves of free chains in Figure 10 indicates eqs 17 and 18 are not changed by merely mixing the particles and the oligomers. It agrees with results of Picu et al.[29] on coarse-grained models that the fillers in nanocomposites elongate the relaxation time of each mode but do not change its dependence on p. Neither eq 17 nor eq 18 is valid if grafting is introduced. It is also interesting to note that, at short time scales, grafted chains relax faster than the free chains at low temperature (top panel of Figure 10), but when the temperature is raised, the relaxation of free chains will eventually become faster (bottom panel of Figure 10). The crossover features of the chains remind us of the same opposite trends of particle diffusions and system viscosities mentioned in sections 3.2 and 3.3. In other words, the enhanced correlation between particles and chains by grafting does not only promote

dx.doi.org/10.1021/jp2112582 | J. Phys. Chem. B 2012, 116, 2385−2395

particle diffusion but also helps prevent damping of chain dynamics as the temperature is lowered. Beside its function as a shield against aggregation, grafting accelerating the dynamics of both particles and chains may be another explanation of the experimentally fluidlike rheology for NOHMs.

4. CONCLUSIONS

The aim of this work is to analyze the predictive ability of an atomistic model for viscosity and diffusivity of a new class of materials—NOHMs. By studying the dynamics of nanoparticles and chains, we also seek to understand the origins of liquidlike behavior of NOHMs observed experimentally. The model developed in this work is based on a combination of integrated LJ potentials for nanoparticles and modified TraPPE force fields for poly(ethylene oxide) oligomers. The model viscosities for POSS-PEO systems, obtained by temperature extrapolation, are of the same order of magnitude as the available experimental data. Our results also show the Stokes−Einstein relation holds for NOHMs (grafted nanoparticle) systems if the solvent is considered to be other NOHMs particles, but does not hold for nanocomposites (ungrafted particles in a medium of chains), because of strong interparticle aggregation. Counterintuitively, at low temperatures increasing chain length increases particle mobilities and reduces the system viscosities. We have also shown that the low molecular weight of chains used in experiments is not a factor explaining the liquidlike behavior of NOHMs. On the contrary, we find that increasing chain length reduces the volume fractions of nanoparticles and therefore reduce the viscosities at low temperatures. Finally, for chains of the same length, both particles and oligomer motions in grafted systems are more mobile than for their ungrafted counterparts as the temperature drops. This indicates that grafting is the main cause for the observed high fluidity of NOHMs systems.

Transport properties of nanoparticle−polymer composites have not previously been obtained from direct simulations. Future improvements of the accuracy of the model can be attempted as follows. First, the integrated LJ potentials may not be the optimal choice for describing nanoparticles comprised by multiple types of atoms. Simulations of pure nanoparticles need to be performed to develop a better coarse-grained representation of particle−particle interactions. In addition, our results show that grouping the atoms in the particles into a solid sphere generates slip boundary conditions for its surface. Prior studies[47,85] argued that it may be an inappropriate method to represent nanoparticles as spheres, because the simplification affects atomistic interactions and thermal motions at the particle surface, which could change the transport properties or rheological boundary conditions (stick/slip) at the surface. Whether this is a significant factor needs to be examined by future work comparing the transport properties of solid-sphere and atomistic grafted nanoparticle systems. Finally, the temperature extrapolations used in this study produce viscosities and diffusivities in fair agreement with those from direct calculations for bulk oligomers. When applying to particle/oligomer systems, they have difficulties capturing temperature-dependent structural transitions. Studies at lower temperatures with the Green−Kubo approach is difficult because of convergence problems. Nonequilibrium methods of viscosity calculation may be worth exploring at low temperatures, provided that sufficiently low perturbations of the equilibrium structures can be maintained.

Our work shows grafting of nanoparticles to chains has two main effects relative to the corresponding ungrafted systems, namely, it reduces particle aggregation and increases particle−oligomer correlations. Our present model can not distinguish the individual contribution of each effect to the decreased viscosity of NOHMs. Some researchers[6] suggest that, as long as the particles are well dispersed, nanocomposites behave like liquids. However, the way particle aggregation was prevented in ref 6 was by grafting polymers to the particles, which introduces both effects. Another possibility would be to use computer simulations with appropriate polymer−particle interactions to realize a nanocomposite system with dispersed particles. Simulations of NOHMs systems with identical interactions as for the dispersed nanocomposite system can then be used to study the effects of particle-chain correlations in the absence of aggregation.

AUTHOR INFORMATION

Corresponding Author

*E-mail: azp@princeton.edu.

Notes

The authors declare no competing financial interest.

ACKNOWLEDGMENTS

This publication was based on work supported by Award No. KUS-C1-018-02, made by King Abdullah University of Science and Technology (KAUST). Simulations were performed primarily on the Della cluster of the TIGRESS High Performance Computing Center at Princeton University. The authors would like to thank Profs. Emmanuel Giannelis, Lynden Archer, Donald Koch, Fernando Escobedo, Alissa Park, and Dr. Alexandros Chremos for helpful discussions and Praveen Agarwal and Kun-Yi Andrew Lin for providing us with viscosity data.

REFERENCES

(1) Koo, J. H. *Polymer Nanocomposites: Processing, Characterization, and Applications*; McGraw-Hill: New York, 2006.
(2) Tiong, S. C. *Mater. Sci. Eng.* **2006**, *53*, 73−197.
(3) Hall, L. M.; Jayaraman, A.; Schweizer, K. S. *Curr. Opin. Solid State Mater. Sci.* **2010**, *14*, 38−48.
(4) Zeng, Q. H.; Yu, A. B.; Lu, G. Q. *Prog. Polym. Sci.* **2008**, *33*, 191−269.
(5) Mackay, M. E.; Tuteja, A.; Duxbury, P. M.; Hawker, C. J.; Horn, B. V.; Guan, Z. B.; Chen, G. H.; Krishnan, R. S. *Science* **2006**, *311*, 1740−1743.
(6) Akcora, P.; Kumar, S. K.; Sakai, V. G.; Benicewicz, B. C.; Schadler, L. S. *Macromolecules* **2010**, *43*, 8275−8281.
(7) Zhang, Q.; Archer, L. A. *Langmuir* **2002**, *18*, 10435−10442.
(8) Akcora, P.; Liu, H. J.; Kumar, S. K.; Moll, J.; Li, Y.; Benicewicz, B. C.; Schdaler, L. S.; Acehan, D.; Panagiotopoulos, A. Z.; Pryamitsyn, V.; Ganesan, V.; Ilavsky, J.; Thiyagarajan, P.; Colby, R. H.; Douglas, J. F. *Nat. Mater.* **2009**, *8*, 354−359.
(9) Pryamtisyn, V.; Ganesan, V.; Panagiotopoulos, A. Z.; Liu, H. J.; Kumar, S. K. J. *Chem. Phys.* **2009**, *131*, 221102.
(10) Martin, T. B.; Seifpour, A.; Jayaraman, A. *Soft Matter* **2011**, *7*, 5952−5964.
(11) Lin, Y. L.; Chiou, C. S.; Kumar, S. K.; Lin, J. J.; Sheng, Y. J.; Tsao, H. K. *J. Phys. Chem. C* **2011**, *115*, 5566−5577.
(12) Kalra, V.; Escobedo, F.; Joo, Y. L. *J. Chem. Phys.* **2010**, *132*, 024901.
(13) Agarwal, P.; Archer, L. A. *Phys. Rev. E* **2011**, *83*, 041402 The paper includes only the data for SiO2-PI NOHMs, but its supplement information presents rheological data for SiO2-PEG NOHMs.

Viscosity data of the self-suspended SiO2-PEG NOHMs are from private communication.
(14) Nugent, J.; Moganty, S. S.; Archer, L. A. *Adv. Mater.* **2010**, *22*, 3677−3680.
(15) Vaia, R. A.; Giannelis, E. P. *Macromolecules* **1997**, *30*, 7990−7999.
(16) Star, F. W.; Douglas, J. F.; Glotzer, S. C. *J. Chem. Phys.* **2003**, *119*, 1777−1788.
(17) Brown, D.; Marcadon, V.; Mélé, P.; Albérola, N. D. *Macromolecules* **2008**, *41*, 1499−1511.
(18) Marla, K. T.; Meredith, J. C. *Langmuir* **2004**, *20*, 1501−1510.
(19) Balazs, A. C.; Ginzburg, V. V.; Qiu, F.; Peng, G. W.; Jasnow, D. *J. Phys. Chem. B* **2000**, *104*, 3411−3422.
(20) Ginzburg, V. V.; Gendelman, O. V.; Manevitch, L. I. *Phys. Rev. Lett.* **2001**, *86*, 5073−5075.
(21) Ndoro, T. V. M; Voyiatzis, E; Ghanbari, A.; Theodorou, D. N.; Böhm, M. C.; Müller-Plathe, F. *Macromolecules* **2011**, *44*, 23162327.
(22) Kalb, J.; Dukes, D.; Kumar, S. K.; Hoy, R. S.; Grest, G. S. *Soft Mater* **2011**, *7*, 1418−1425.
(23) Nair, N.; Wentzel, N.; Jayaraman, A. *J. Chem. Phys.* **2011**, *134*, 194906.
(24) Nair, N.; Jayaraman, A. *Macromolecules* **2010**, *43*, 8251−8263.
(25) Jayaraman, A.; Schweizer, K. S. *Macromolecules* **2009**, *42*, 8423−8434.
(26) Barbier, D.; Brown, D.; Grillet, A.-C.; Neyertz, S. *Macromolecules* **2004**, *37*, 4695−4710.
(27) Brown, D.; Mélé, P.; Marceau, S.; Albérola, N. D. *Macromolecules* **2003**, *36*, 1395−1406.
(28) Vladkov, M.; Barrat, J. L. *Macromolecules* **2007**, *40*, 3797−3804.
(29) Picu, R. C.; Rakshit, A. *J. Chem. Phys.* **2007**, *126*, 144909.
(30) Fujii, Y.; Yang, Z. H.; Clough, A.; Tsui, O. K. C. *Macromolecules* **2010**, *43*, 4310−4313.
(31) Odegard, G. M.; Clancy, T. C.; Gates, T. S. *Polymer* **2005**, *46*, 553−562.
(32) Lacevic, N.; Gee, R. H.; Saab, A.; Maxwell, R. *J. Chem. Phys.* **2008**, *129*, 124903.
(33) Knauert, S. T.; Douglas, J. F.; Starr, F. W. *J. Polym. Sci., Part B: Polym. Phys.* **2007**, *45*, 1882−1897.
(34) Smith, G. D.; Bedrov, D.; Li, L.; Byutner, O. *J. Chem. Phys.* **2002**, *117*, 9478−9489.
(35) Liu, J.; Cao, D. P.; Zhang, L. Q. *J. Phys. Chem. C* **2008**, *112*, 6653−6661.
(36) Yu, H.-Y.; Koch, D. L. *Langmuir* **2010**, *26*, 16801−16811.
(37) Chremos, A.; Panagiotopoulos, A. Z. *Phys. Rev. Lett.* **2011**, *107*, 105503.
(38) Chremos, A.; Panagiotopoulos, A. Z.; Yu, H.-Y.; Koch, D. L. *J. Chem. Phys.* **2011**, *135*, 114901.
(39) Chremos, A.; Panagiotopoulos, A. Z.; Koch, D. L. *J. Chem. Phys.* **2012**, in press.
(40) Lin, K.-Y.; Park, A.-H. A. *Environ. Sci. Technol.* **2011**, *45*, 6633−6639 The paper does not present the rheological data for any of the samples. The viscosity data of NP-NOHM-C-HPE (silica NP, 2 nm diameter), POSS-NOHM-C-HPE and POSS-PEG are from private communication.
(41) Goyal, S.; Escobedo, F. A. *J. Chem. Phys.* **2011**, *135*, 184902.
(42) Affouard, F.; M. Descamps, L.-C. V.; Habasaki, J.; Bordat, P.; Ngai, K. L. *J. Chem. Phys.* **2009**, *131*, 104510.
(43) Mallamace, F.; Branca, C.; Corsaro, C.; Leone, N.; Spooren, J.; Stanley, H. E.; Chen, S.-H. *J. Phys. Chem. B* **2010**, *114*, 1870−1878.
(44) Harris, K. R. *J. Chem. Phys.* **2009**, *131*, 054503.
(45) Wachter, P.; Zistler, M.; Schreiner, C.; Fleischmann, M.; Gerhard, D.; Wasserscheid, P.; Barthel, J.; Gores, H. J. *J. Chem. Eng. Data* **2009**, *54*, 491−497.
(46) McCabe, M.; Maguire, D. J.; Lintell, N. A. *Adv. Exp. Med. Biol.* **2005**, *566*, 143−149.
(47) Li, Z. G. *Phys. Rev. E* **2009**, *80*, 061204.
(48) Brochard-Wyart, F.; deGennes, P. G. *Eur. Phys. J. E* **2000**, *1*, 93−97.
(49) deGennes, P. G. *Rev. Mod. Phys.* **1985**, *57*, 827−863.
(50) Yamamoto, U.; Schweizer, K. S. *J. Chem. Phys.* **2011**, *135*, 224902.
(51) Cai, L.-H.; M. Rubinstein, S. P. *Macromolecules* **2011**, *44*, 7853−7863.
(52) Tuteja, A.; Mackay, M. E.; Narayanan, S.; Asokan, S.; Wong, M. S. *Nano Lett.* **2007**, *7*, 1276−1281.
(53) Alter, B. J.; Gass, D. M.; Wainwright, T. E. *J. Chem. Phys.* **1970**, *53*, 3813−3826.
(54) Vergeles, M.; Keblinski, P.; Koplik, J.; Banavar, J. R. *Phys. Rev. E* **1996**, *53*, 4852−4864.
(55) Rodriguez, R.; Herrera, R.; Archer, L. A.; Giannelis, E. P. *Adv. Mater.* **2008**, *20*, 4353−4358.
(56) Calahorra, E.; Cortazar, M.; Guzman, G. M. *J. Polym. Sci.: Polymer. Lett. Ed.* **1985**, *23*, 257−260.
(57) Gurman, J. L.; Baier, L.; Levin, B. C. *Fire Mater.* **1987**, *11*, 109−130.
(58) Doi, M.; Edwards, S. F. *The Theory of Polymer Dynamics*; Oxford University: New York, 1986.
(59) Hunter, R. J. *Foundations of Colloid Science*, 2nd ed.; Oxford University: New York, 2001.
(60) Hamaker, H. C. *Physica* **1937**, *4*, 1058−1072.
(61) Everaers, R.; Ejtehadi, M. R. *Phys. Rev. E* **2003**, *67*, 041710.
(62) in't Veld, P. J.; M. A. Horsch, J. B. L.; Grest, G. S. *J. Chem. Phys.* **2008**, *129*, 164504.
(63) Fischer, J.; Paschek, D.; Geiger, A.; Sadowski, G. *J. Phys. Chem. B.* **2008**, *112*, 2388−2398.
(64) Hong, B. B.; Fernando, E.; Panagiotopoulos, A. Z. *J. Chem. Eng. Data* **2010**, *55*, 4273−4280.
(65) Plimpton, S. J. *J. Comput. Phys.* **1995**, *117*, 1−19.
(66) LAMMPS Users Manual. http://lammps.sandia.gov/.
(67) Perchak, D.; Skolnick, J.; Yaris, R. *Macromolecules* **1985**, *18*, 519−525.
(68) Hsieh, C.-C.; Jain, S.; Larson, R. G. *J. Chem. Phys.* **2006**, *124*, 044911.
(69) Stubbs, J. M.; Potoff, J. J.; Siepmann, J. I. *J. Phys. Chem. B.* **2004**, *108*, 17596−17605.
(70) Rodriguez, R.; Herrera, R.; Bourlinos, A. B.; Li, R. P.; Amassian, A.; Archer, L. A.; Giannelis, E. P. *Appl. Organometal. Chem.* **2010**, *24*, 581−589.
(71) Allen, M. P.; Tildesley, D. J. *Computer Simulation of Liquids*; Oxford University: New York, 1987.
(72) http://www.chemical-buyers.com/cas-107/1072-40-8.html.
(73) Conesa, A.; Shen, S.; Coronas, A. *Int. J. Thermophys.* **1998**, *19*, 1343−1358.
(74) Zoller, P.; Walsh, D. J. *Standard Pressure-Vol.-Temperature Data for Polymers*; Technomic Pub: Lancaster, PA, 1995.
(75) Swier, S.; Pieters, R.; van Mele, B. *Polymer* **2002**, *43*, 3611−3620.
(76) de Gennes, P. G. *Adv. Colloid Interface Sci.* **1987**, *27*, 189−209.
(77) Fischer, J.; Paschek, D.; Geiger, A.; Sadowski, G. *J. Phys. Chem. B* **2008**, *112*, 13561−13571.
(78) Janzen, J. *J. Appl. Phys.* **1975**, *46*, 966−969.
(79) Rey-Castro, C.; Vega, L. F. *J. Phys. Chem. B* **2006**, *110*, 14426−14435.
(80) Poling, B. E.; Prausnitz, J. M.; O'Connell, J. P. *The Properties of Gases and Liquids*, 5th ed.; McGraw-Hill: New York, 2001.
(81) http://www.hybridplastics.com/products/pg1190.htm.
(82) Agarwal, P.; Qi, H. B.; Archer, L. A. *Nano Lett.* **2010**, *10*, 111−115.
(83) Every, H. A.; Bishop, A. G.; MacFarlane, D. R.; Orädd, G.; Forsyth, M. *Phys. Chem. Chem. Phys.* **2004**, *6*, 1758−1765.
(84) Leutheusser, E. *Phys. Rev. A* **1984**, *29*, 2765−2773.
(85) Li, Z. G.; Wang, H. *Phys. Rev. Lett.* **2005**, *95*, 014502.